Supplementary information

High ionic conductivity with low degradation in A-site strontium doped non-stoichiometric sodium bismuth titanate perovskite

Fan Yang, Huairuo Zhang, Linhao Li, Ian M. Reaney and Derek C. Sinclair*
Department of Materials Science and Engineering, University of Sheffield, Sir Robert Hadfield Building, Mappin Street, Sheffield, S1 3JD, UK.

* Author to whom correspondence should be addressed.
Email: d.c.sinclair@sheffield.ac.uk

Methods

Sr-doped $NB_{0.49}T$ ceramics were prepared by a solid state reaction method using Na_2CO_3 (99.5%, Fisher chemical, UK), Bi_2O_3 (99.9%, Acros Organics, USA), TiO_2 (99.9%, Sigma Aldrich, UK) and $SrCO_3$ (99.9%, Sigma Aldrich, UK) as starting materials. Prior to weighing, the raw powders were dried overnight at 300 ºC for Na_2CO_3 and Bi_2O_3, 180 ºC for $SrCO_3$ and 800 ºC for TiO_2. Appropriate amounts of each precursor were weighed and mixed thoroughly in iso-propanol using yttria-stabilised zirconia grinding media for 6 hours. The mixture was dried overnight at 85 °C, sieved and then calcined at 800 °C for 2 hours. The resultant powders were subjected to a second round of ball milling, drying, sieving and calcination and subsequently to a final, third round of ball milling and sieving. The products were compacted into pellets by uni-axial cold pressing using poly vinyl alcohol (PVA) as a binder. Pellets were embedded in sacrificial powder of the same composition and sintered at 1150 °C for 2 hours after decomposing the binder at 550 °C for 2 hours. For comparison, $(Bi_2O_3)_{0.8}(Er_2O_3)$, 20ESB and $(BiO_{1.5})_{0.88}(DyO_{1.5})_{0.08}(WO_3)_{0.04}$, 8D4WSB, were also prepared by the solid state reaction method using Bi_2O_3 (99.9%, Acros Organics, USA), Er_2O_3 (99.9%, Stanford Advanced Materials, USA), Dy_2O_3 (99.9%, Stanford Advanced Materials, USA) and WO_3 (99.8%, Alfa Aesar, UK). Calcination and sintering temperatures were 800 °C and 925 °C, respectively.

Ceramic density was measured by the Archimedes' method and compared to the theoretical X-ray density. Phase purity was established by X-ray diffraction on crushed pellets using a high resolution STOE STADI-P diffractometer (STOE & Cie GmbH, Darmstadt, Germany) operating with $CuK\alpha_1$ radiation with a linear position-sensitive

detector. The crushed pellets were annealed at 400 ºC for 4 hours to eliminate any residual stress caused by crushing and grinding. Lattice parameters were calculated from structural refinement for reflections in the range of $10º \leq 2\theta \leq 100º$ using EXPGUI [1, 2]. Ceramic microstructures were observed by scanning electron microscopy (JEOL JSM-6010LA, JEOL Ltd., Tokyo, Japan) on thermally etched surfaces. Compositions were obtained by energy dispersive X-ray spectroscopy (EDX) on polished samples (without thermal etch). Electron transparent transmission electron microscopy (TEM) specimens were prepared by mechanical polishing and dimpling to a thickness of less than 10 μm followed by Ar ion-milling in a Gatan precision ion polishing system (PIPS). TEM in-situ heating experiments were performed using a JEOL 2010 transmission electron microscope (JEOL Ltd., Tokyo, Japan) operated at 200 keV. Selected area electron diffraction patterns (SAEDPs) were collected using a CCD camera.

Electrical properties were measured by high temperature impedance spectroscopy using an Agilent E4980A impedance analyser (Agilent Technologies Inc., Palo-Alto, CA) or a Solartron 1260 system (Solartron Analytical, UK) using Au paste (fired at 800 °C for 2 h) as electrodes. All impedance data were corrected for high frequency inductance associated with the leads and the measurement jig by performing a short circuit measurement and normalised by a geometric factor (thickness/surface area). Equivalent circuit fitting was performed using ZView software (Scribner Associates, Inc, Southern Pines, NC). Oxygen-ion transport number measurements were performed using a Probostat system (NorECs Norwegian Electro Ceramics AS, Oslo, Norway). A sample was sealed onto a YSZ tube using a commercial glass frit. An oxygen partial pressure (pO_2) difference was created across the ceramic by flowing N_2 into the YSZ tube and leaving the outside of the ceramic in air. The pO_2 difference was monitored by measuring the voltage across the inner and outer electrodes on the YSZ tube. The voltage was measured using a Keithley 182 sensitive digital voltmeter.

XRD and SEM

Sr-doped $NB_{0.49}T$ was phase-pure by XRD. The structure was refined to a rhombohedral cell (space group: *R3c*) with lattice parameters of $a = 0.5492$ and $c = 1.3497$ nm. An SEM image on a thermally etched surface revealed a dense body and an average grain size of ~ 5 μm. EDX analysis on Sr-doped $NB_{0.49}T$ shows the Na percentage remains almost identical to undoped $NB_{0.49}T$, whereas the Bi percentage decreases. This confirms the doping mechanism

being $Sr^{2+} \rightarrow Bi^{3+} + \frac{1}{2}O^{2-}$. The Ti percentage in both samples (~ 49.0 %) is slightly lower but within 2 or 3 standard deviations of the theoretical value (50.0 %).

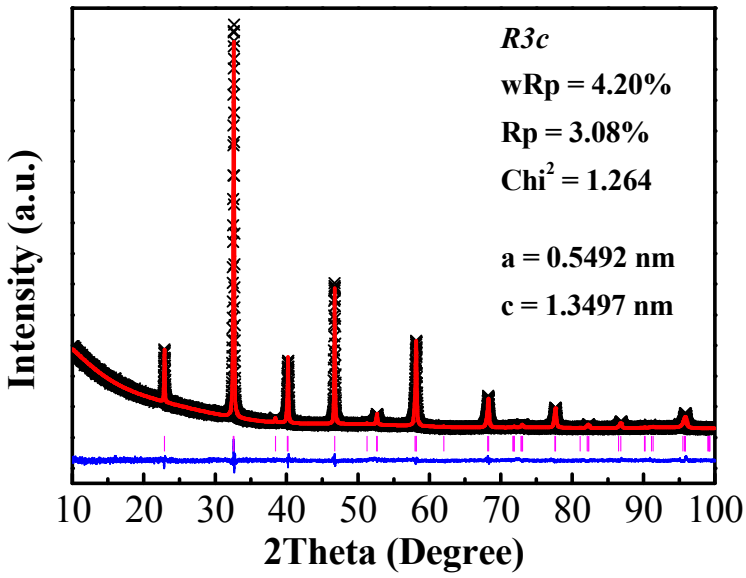

Figure S1 XRD pattern and Rietveld refinement of Sr-doped $NB_{0.49}T$. The cross symbols represent the observed pattern and the solid line shows the calculated fit. The reflection marker for the R*3c* structure is shown as vertical lines with the difference pattern below the diffraction pattern. The quality of fit and lattice parameters are indicated in the figure.

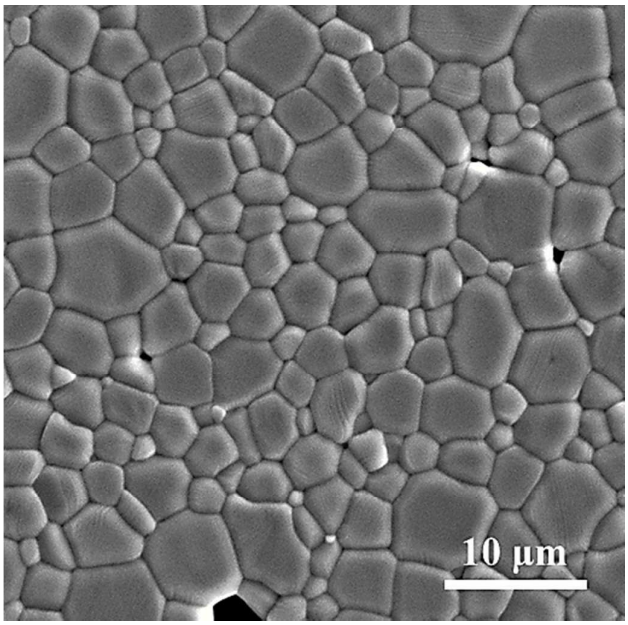

Figure S2 SEM micrograph of a thermally etched surface of a Sr-doped $NB_{0.49}T$ ceramic.

Table S1 Analysed composition of undoped and Sr-doped $NB_{0.49}T$ ceramics determined by EDX. Data were collected from 10 randomly selected areas on polished surfaces (without thermal etch).

Starting composition	Na (at.%)	Bi (at.%)	M (at.%)	Ti (at.%)
$NB_{0.49}T$	25.9 (± 0.2)	25.1 (± 0.3)	N/A	49.0 (± 0.2)
Sr-doped $NB_{0.49}T$	25.6 (± 0.3)	24.3 (± 0.3)	1.1 (± 0.3)	49.0 (± 0.3)

Impedance spectroscopy and equivalent circuit fitting

A typical complex impedance plane (Z*) plot of these ceramics showed three arcs (Figure S3a). From high to low frequency (left to right), they represent the response from the grains (bulk), grain boundaries and electrode effects, respectively. An equivalent circuit of three resistor-constant phase elements (R-CPE) connected in series (inset figure) was used to fit the data. The impedance residuals, defined as $Z_{residual} = (Z_{measured} - Z_{fitted})/|Z_{measured}|$, are used to present the difference between the measured and fitted data. The impedance residuals are less than 2% within the frequency range (Figure S3b), indicating the validity of the selected equivalent circuit and to give confidence in the extracted resistance values.

Impedance measurements were also carried out in flowing nitrogen, air and oxygen atmospheres. The bulk conductivity was independent of the oxygen partial pressure (pO_2), as shown in Figure S4. The pO_2-independent conductivity supports the suggestion that the electrical conduction is predominately ionic over the limited T-pO_2 range investigated.

The predominate ionic conduction in Sr-$NB_{0.49}T$ was confirmed by EMF measurements that revealed an ionic transport number, t_i, > 0.9 at 600 – 700 °C, dropping to ~ 0.88 at 800 °C. These values are similar to those reported for undoped and Mg-doped $NB_{0.49}T$ [3].

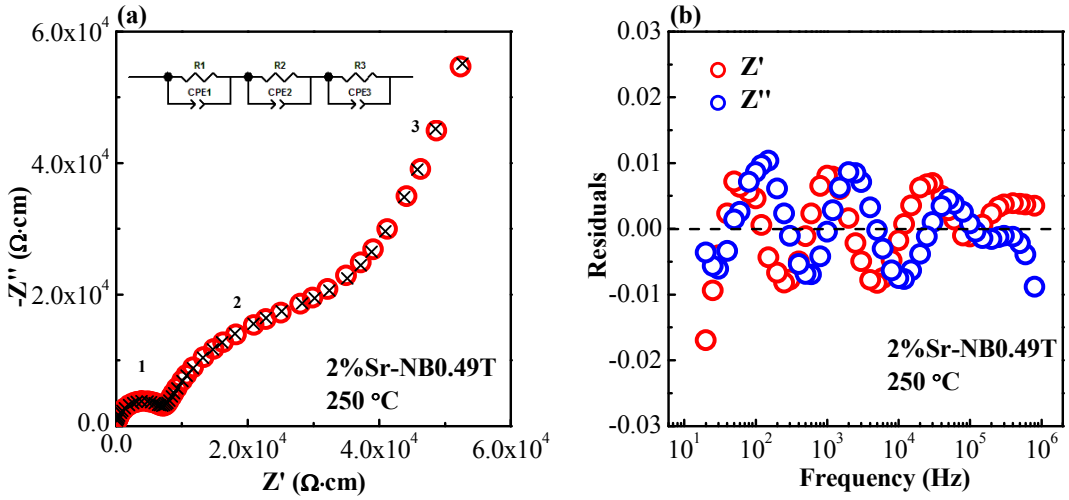

Figure S3 (a) A complex impedance (Nyquist) plot of Sr-doped $NB_{0.49}T$ ceramic measured at 250 °C in air. The inset figure is the equivalent circuit used to model the data; (b) Impedance residuals versus frequency showing the quality of fit.

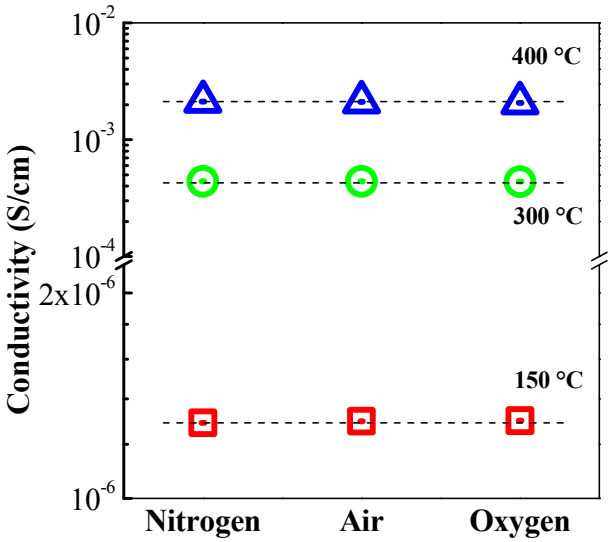

Figure S4 Bulk conductivity of Sr-doped $NB_{0.49}T$ ceramic measured in air, nitrogen and oxygen at 150, 300 and 400 °C.

Table S2 Oxygen ion transport number of Sr-doped, Mg-doped and undoped $NB_{0.49}T$.

	600 °C	700 °C	800 °C
$NB_{0.49}T$ [3]	0.93	0.92	0.89
Mg-doped $NB_{0.49}T$ [3]	0.98	0.95	0.93
Sr-doped $NB_{0.49}T$	0.96	0.94	0.88

Variable temperature TEM

Selected area electron diffraction patterns (SAEDPs) were recorded from room temperature to ~400 °C. An SAEDP recorded at 310 °C along the pseudocubic $[013]_p$ zone-axis is shown in Figure S5 and clearly shows the coexistence of rhombohedral and tetragonal phases in $NB_{0.49}T$ at this temperature. The diffraction spots are indexed with the pseudocubic structure. The white and black arrows illustrate the superlattice diffraction spots arising from TiO_6 octahedral tilting. The ½{*eoo*} (where *o* = odd and *e* = even) spots mainly arise from $a^0a^0c^+$ in-phase tilting (tetragonal structure, *P4bm*), and the ½{*ooo*} spots from $a^-a^-a^-$

antiphase tilting (rhombohedral structure, *R3c*). The rhombohedral and tetragonal phases intergrow and coexist in NBT materials over a wide temperature range and this will be fully reported elsewhere [5]. The coexistence/intergrowth of the R and T phases gives rise to tilt disorder at the R/T interface resulting in additional streaking along the [100] direction.

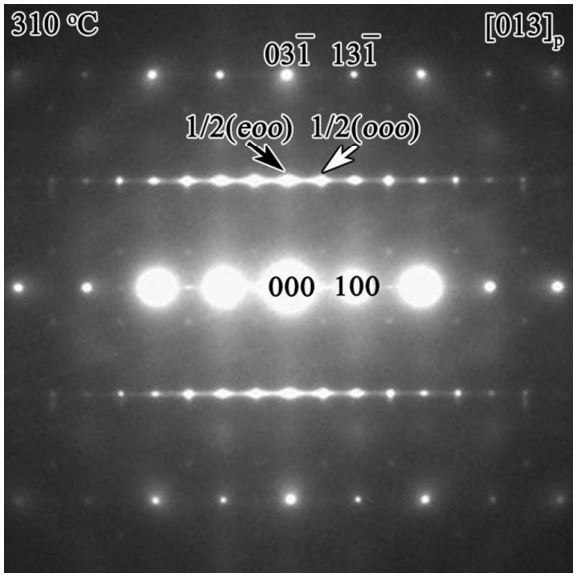

Figure S5 Electron diffraction pattern of $NB_{0.49}T$ at 310 ^{o}C showing the co-existence of rhombohedral and tetragonal phases.

Fitting of bulk conductivity at 250 – 400 °C using the Maxwell model

In the temperature range ~ 250 - 400 °C, $NB_{0.49}T$-based ceramics were considered as a composite of two polymorphic phases (rhombohedral, R and tetragonal, T). The bulk conductivity of each phase, σ(R) and σ(T), was obtained by extrapolating the low temperature σ_b (< 250 °C) and the high temperature σ_b (> 400 °C) data, respectively to the range ~ 250 to 400 °C. The conductivity of the two-phase composite was estimated using the Maxwell model $\sigma = \sigma_1 \frac{2\sigma_1 + \sigma_2 + 2x_2(\sigma_2 - \sigma_1)}{2\sigma_1 + \sigma_2 - x_2(\sigma_2 - \sigma_1)}$, where the subscripts *1* and *2* represent R and T phases, respectively and *x* represents the volume fraction. Here we employed the *x* values from Ref.[4] based on the assumptions that such a low level of Bi non-stoichiometry and a low Sr-doping level do not dramatically change the phase transformation temperatures and volume

fractions of NBT materials. The predicted conductivity by the Maxwell model fits the experimental data reasonably well, as shown in Figure S6.

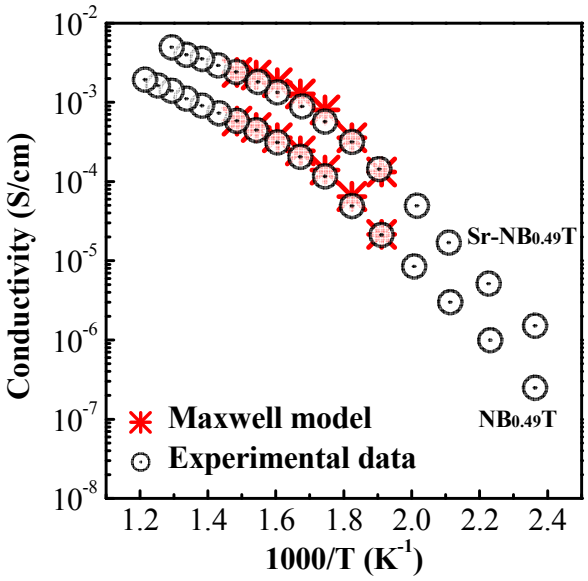

Figure S6 Arrhenius plot of σ_b for $NB_{0.49}T$ and Sr-doped $NB_{0.49}T$. Circle symbols are experimental data, and the cross symbols are calculated based on a rhombohedral and tetragonal two-phase mixture using the Maxwell model.

Acknowledgement

We thank the EPSRC for funding EP/L027348/1.

Reference

[1] Larson A. C.; Von Dreele R. B. General Structure Analysis System (GSAS). Los Alamos National Laboratory Report LAUR **1994**, 86-748.

[2] Toby B. H. EXPGUI, a graphical user interface for GSAS. J. Appl. Crystallogr. **2001**, 34, 210-213.

[3] Li M; Pietrowski M. J.; De Souza R. A.; Zhang H; Reaney I. M.; Cook S. N.; Kilner J. A.; Sinclair D. C. A family of oxide ion conductors based on the ferroelectric perovskite $Na_{0.5}Bi_{0.5}TiO_3$. Nat. Mater. **2014**, 13, 31-35.

[4] Jones G. O.; Thomas P. A. Investigation of the structure and phase transitions in the novel A-site substituted distorted perovskite compound $Na_{0.5}Bi_{0.5}TiO_3$. Acta Crystallogr., Sect. B **2002**, 58, 168-178.

[5] Zhang H; Li M; Li L; Yang F; Trolier-McKinstry S.; Sinclair D. C.; Reaney I. M. manuscript in preparation.